processes

MDPI

Article

Design and Performance of Nonlinear Control for an Electro-Hydraulic Actuator Considering a Wearable Robot

Buchun Song, Dongyoung Lee, Sang Yong Park and Yoon Su Baek *

Department of Mechanical Engineering, Yonsei University, Seoul 03722, Korea; theme7749@gmail.com (B.S.); frh1024@naver.com (D.L.); parksy@yonsei.ac.kr (S.Y.P.)

* Correspondence: ysbaek@yonsei.ac.kr; Tel.: +82-2-2123-2827

Received: 30 May 2019; Accepted: 18 June 2019; Published: 21 June 2019

Abstract: In the development of a wearable robot, compact volume size, high energy efficiency, and a high load capacity linear actuator system are necessary. However, conventional hydraulic actuator systems are difficult to apply to wearable robots. Also, they have nonlinearities because of the presence of hydraulic fluid in a single rod cylinder. Electric linear actuators resolve the problems of hydraulic systems. However, due to their low load capacity, they are not easy to apply to wearable robots. In this paper, a pump-controlled electro-hydraulic actuator (EHA) system that considers the disadvantages of the hydraulic actuator and electric actuator is proposed for a wearable robot. Initially, a locking circuit design is considered for the EHA to give the system load holding capacity. Based on the developed model, the adaptive sliding mode control (ASMC) scheme is designed to resolve the nonlinearity problem of changes in the dynamic system. The ASMC scheme is then modeled and verified with Simulink. In order to verify the performance of the proposed adaptive control with the model, experiments are conducted. The proposed EHA verifies that the ASMC reaches the target value well despite the existence of many model uncertainties.

Keywords: pump-controlled electro-hydraulic actuator; adaptive sliding mode control; locking circuit design

1. Introduction

Conventional hydraulic actuators have commonly been used in plenty of heavy equipment applications. Examples include the use of excavators and dozers in the construction industry, offshore drilling and marine machinery in the marine industry, active suspension systems in the automotive industry, and wearable robots in the medical device industry [1–3]. According to one survey that addressed longer lifespans, the dependency of wearable robots using linear actuators should be increased, given the related increase in human life expectancy [4]. Therefore, it is important for more studies to focus on increasing muscular strength using actuators, such as with wearable robots for rehabilitation training, in military applications, and in commercial applications. For hydraulic actuators, there are generally two ways to control a system: with a controlled pump or with a controlled valve. Controlled pumps have slow responses because the contained volumes are large, and the pressure must be built up initially. However, the pressure levels of both the lines and the flow are closely matched to the load requirements, resulting in much higher energy efficiency [5]. On the other hand, controlled valves offer rapid responses because the contained volumes are small. Nonetheless, regardless of the load pressure, the energy efficiency is low because the supply pressure is constant, and internal leakages occur when changing the direction of the fluid in the valve [6,7]. Despite these disadvantages, the conventional hydraulic system is widely used in heavy industries due to its high

power and torque ratios, rapid responses, and excellent heat resistance [8]. However, mainly due to the low energy efficiency, fluid leakages from valves, large volume size, and limited installation space, the application of wearable robots is limited. Additionally, because hydraulic fluid is the main energy medium in the system, the system contains uncertain fluid parameters in hydraulic control. On the other hand, electric linear actuators have distinct advantages over hydraulic actuators in terms of their simplicity and their highly efficient energy usage, but their poor load holding capabilities continue to be a problem. For example, electric linear actuators constantly consume energy to maintain the current positional holding of a heavy weight. As a result, the energy efficiency is reduced. Wearable robots are also associated with related safety issues. For instance, the driving force of electric linear actuators is controlled by the torque force of a motor. However, if the power of the motor fails, a wearable robot may be damaged due to its heavy weight. In addition, they are not as cost-effective as hydraulic actuators in terms of their power and torque ratios [9]. Therefore, the development of a much more flexible system that is applicable to multiple areas is required to meet the rapidly changing demands of current technologies.

The development of an electro-hydraulic actuator (EHA) utilizing a hydraulic system with electrical power is one solution that may overcome these drawbacks [10]. EHAs can be operated with either pump-controlled or valve-controlled approaches, and they are considered to be more flexible systems. The pump-controlled EHA allows direct position adjustments, and when reaching the target value, the constant supply pressure is stopped. As a result, the pump-controlled EHA has higher energy efficiency than the conventional hydraulic actuator and the valve-controlled type of EHA [5,9]. However, most EHA studies conducted thus far have focused on valve-controlled EHAs [11–18]; these types offer a quick response, but their energy efficiency is low due to the supply of constant pressure [5]. Due to this constant pressure supply, leakage from the valves increases gradually. This accumulated leakage leads to poor performance due to the introduction of many uncertainties. In addition, the dynamic system changes due to the presence of a single rod cylinder, and uncertain fluid parameters occur in hydraulic control. As a result, these model uncertainties lead to nonlinear systems.

Several approaches have been proposed to resolve the nonlinearity issue associated with valve-controlled EHAs, and many studies have utilized simulations and experiments. For example, Yong Yang, Lei Yong Yang, Lei Ma, and Deqing Huang solved this issue by using valve-controlled EHAs with an exoskeleton that handles loads with the lower limbs based on a backstepping tracking method with feedback learning [11]. Although their controller was verified in a simulation, it is necessary to verify it with actual experiments. In addition, backstepping control, adaptive robust control, adaptive sliding mode control, and pressure feedback have been utilized in experimental efforts to address the nonlinearity issue of valve-controlled EHAs. However, with the valve-controlled method, the double-rod cylinder and single-rod cylinder used are dynamically different and applying the load to the robot leg with the single-rod cylinder was found to be challenging [12–16]. Although non-linear control methods have been demonstrated with valve-controlled EHAs, these systems remain associated with low energy efficiency levels due to leakage problems stemming from the valve characteristics [5–7]. Mostly, given its effectiveness for relatively high-order systems, backstepping or sliding mode control schemes have been utilized to solve these nonlinear uncertain systems. Thus far, studies have focused on adaptive backstepping control, tuning a PID sliding mode controller and a sensor fault-tolerance control design using a pump-controlled EHA [19–21]. With the application of increasingly intelligent systems, energy efficiency becomes more important. Therefore, more advanced studies to improve energy efficiency levels when using pump-controlled EHAs are necessary.

In relation to EHA development, considering a wearable robot, dynamics and safety issues are crucial. In work on system safety, a sensor-fault-tolerant control design for a pump-controlled EHA has been used to maintain system performance [21]. However, fault tolerance control is a software performance, and not a hardware performance issue. Hence, the control will not function properly if the motor completely malfunctions or is turned off. Therefore, this paper presents a means of position control for a pump-controlled electro-hydraulic actuator (EHA) system with an adaptive sliding mode

control scheme and locking circuit design. The proposed circuit design maintains the pressure in the actuator, regardless of an external environment. In other words, even if the motor is stationary or fails, the system is stopped while maintaining the internal pressure in the actuator, thereby preventing damage to the robot and increasing the safety and energy efficiency. The proposed ASMC is used as an error compensation method, with certain nonlinearities related to uncertain fluid parameters and unknown model parameters in a hydraulic control scheme.

In this paper, the design and performance of a pump-controlled EHA are presented considering its use in a wearable robot. The proposed design of the pump-controlled EHA is described, and the EHA performance is verified with Simscape Fluids in Section 2. A controller based on adaptive sliding mode control is presented, and the stability of the system is proved with the Lyapunov theorem in Section 3. The proposed adaptive control scheme is demonstrated by experiments in Section 4. Finally, the conclusions of this paper are presented in the last section.

2. Mathematical Modeling of an Electro-Hydraulic Actuator

The proposed EHA consists of a brushless DC electric motor (BLDC), a bidirectional swash axial piston pump, directional valves, safety valves, a linear variable differential transformer (LVDT), and a 12 cm single rod actuator, which was selected after calculation according to the angle and length of the knee, as shown in Figure 1. There are a total of six directional valves, two of which serve to maintain the constant pressure in the actuator. The remaining four valves are responsible for suction and draining. Two safety valves prevent damage to the actuator, and the pump serves to change the fluid direction.

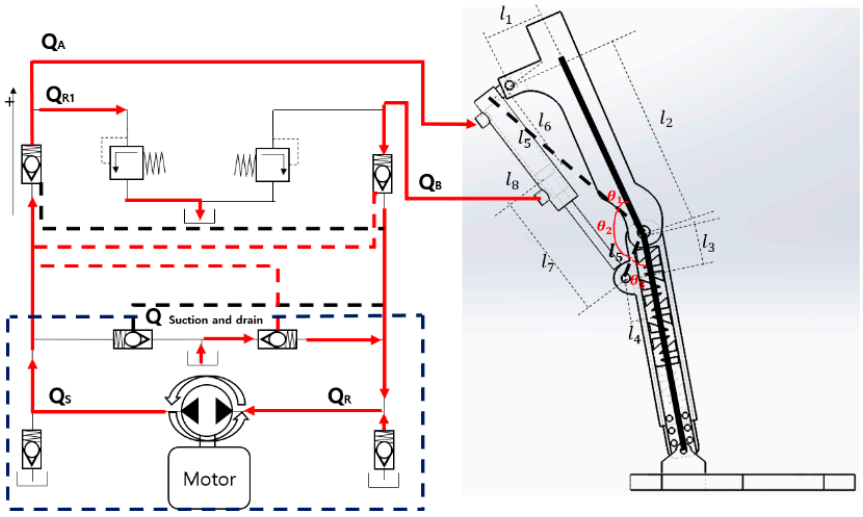

Figure 1. Block diagram of the locking circuit in the pump-controlled EHA system. The locking valves in the locking circuit are located in both hydraulic fluid passages and serve to maintain the pressure in the actuator.

Figure 2 shows a schematic of a swash axial piston pump with the pistons arranged at regular intervals in a cylinder block. There is a swash axial plate, a cylinder block, several assemblies of pistons with a slipper, a valve plate, and a shaft in the pump. The valve plate and swash axial plate are fixed, while the cylinder block is held against the valve plate.

Safety and energy efficiency are important for EHA development considering a wearable robot. The proposed hydraulic circuit can prevent damage to the robot and increase the energy efficiency by two pilot check valves, which are placed on hydraulic lines in Figure 3a. The valves maintain the pressure inside the actuator, regardless of an external environment. Simscape Fluid was used to verify the proposed hydraulic circuit. Figure 3a shows what happens when 1500 rpm is given to the

hydraulic circuit as the input value, and the result of the cylinder position is shown in Figure 3b. The experimental results were gained from the parameters shown in Table 1.

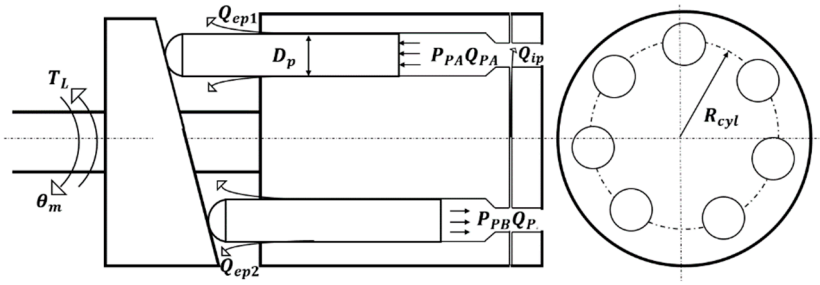

Figure 2. Schematic of a fixed displacement piston pump. The pump consists of a cam, a shaft, a cylinder block, a cylinder valve, and cylinder rods and rod shoes.

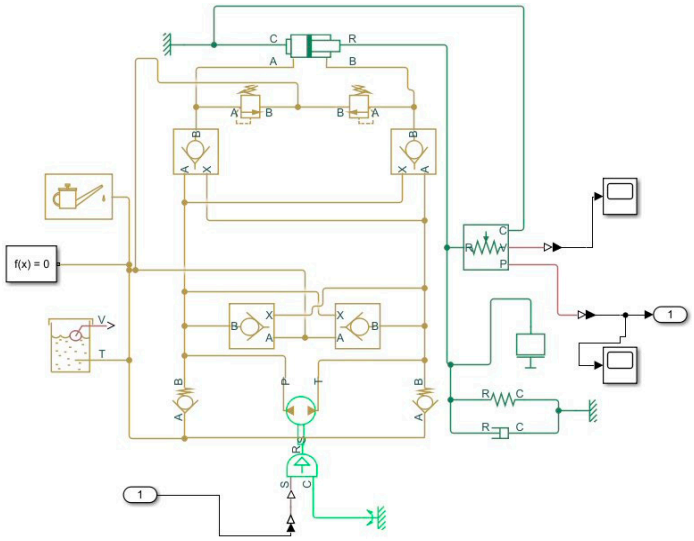

(**a**)

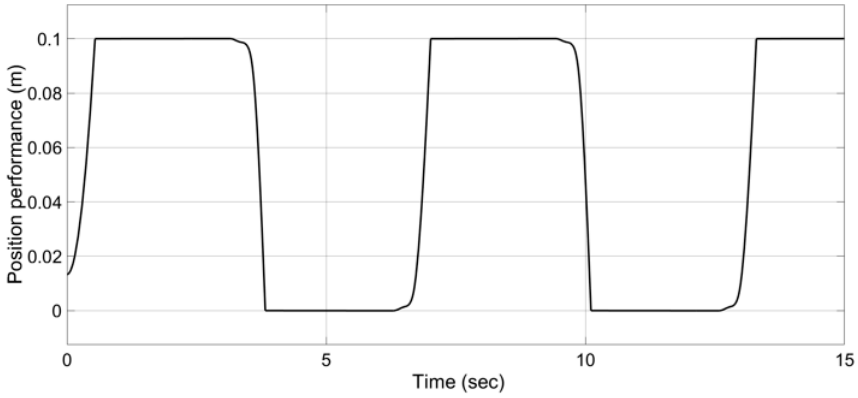

(**b**)

Figure 3. Result of the sine wave in the pump-controlled electro-hydraulic actuator (EHA) without a controller: (**a**) is designed with a hydraulic circuit, and (**b**) is the result of the position performance via Simscape Fluid.

Table 1. Hydraulic Parameters for the electro-hydraulic actuator (EHA) Simulation.

Parameter	Specification
x_c	≤0.125 m
ω	1500 rpm
V_0	0.0001 m^3/s
M	15 kg
β_e	17,200 bar
A	0.2 (N/m)
B	0.05 N/(m/s)
Φ	11.6°
k_p	7

When the motor rotates the shaft, the displacement of the pump volumetric equation can be expressed as follows [22,23]:

$$D_{pv} = \frac{\pi}{4} D_p^2 \, 2R_{cyl} \tan(\varnothing) K_p \tag{1}$$

where D_{pv} is the volumetric displacement of the pump, D_p is the piston diameter in the cylinder block, R_{cyl} is the bore pitch radius of the cylinder block, $\varnothing$ is the swash axial plate angle, and K_p denotes the number of pistons. The pump dynamics of the steady-state continuity equation can be written as in earlier work [5]:

$$\begin{cases} Q_{pA} = D_{pv}\dot{\theta}_m + C_{ep}P_{pA} + C_{ip}(P_{pA} - P_{pB}) \\ Q_{pB} = D_{pv}\dot{\theta}_m - C_{ep}P_{pB} - C_{ip}(P_{pB} - P_{pA}) \end{cases}. \tag{2}$$

The pump is connected by two lines, Q_S and Q_R, in the chambers. Q_{pA} is the forward flow to the Q_S chamber, Q_{pB} is the return flow to the Q_R chamber, and C_{ip} and C_{ep} are the internal and external leakage coefficients, respectively. P_{pA} and P_{pB} represent the pressure levels in the chambers, and D_{pv} and $\dot{\theta}_m$ are the pump volumetric displacement and pump speed, respectively. Subtracting Q_{pB} from Q_{pA} determines the average load flow Q_P:

$$Q_p = D_{pv}\dot{\theta}_m - C_t P_L \tag{3}$$

where

$$\begin{cases} Q_p = \frac{Q_{pA}+Q_{pB}}{2} \\ C_t = \frac{C_{ep}}{2} + C_{ip} \end{cases}.$$

C_t is the total leakage coefficient, and P_L is the pressure difference between P_{pA} and P_{pB}. In the proposed electro-hydraulic actuator (EHA) lock circuit, four pilot valves are used to maintain the actuator pressure or to relieve the pressure. Two check valves are used to supply and return the hydraulic pressure, and two safety valves are used to protect the system from damage due to the occurrence of peak inspiratory pressure. The valve is fully closed when the pressure difference between P_{pA} and P_{pB} is lower than the cracking pressure. Two safety valves are referred to as pressure safety valves. The role of the safety valves is to reduce the pressure when it exceeds the valve pressure setting. When P_{pA} or P_{pB} reaches the cracking pressure, the valve passage area is increased gradually. The valve flow rate is determined by the pressure difference, which can be determined as in earlier work [5]:

$$Q_{check1} = C_d A_s \sqrt{\frac{2\left|P_{pA} - P_{pB}\right|}{\rho\left[\left(P_{pA} - P_{pB}\right)^2 + P_{\mathrm{cr}}^2\right]^{1/4}}}, \; Q_{safety1} = C_d A_s \sqrt{\frac{2}{\rho}} \frac{\Delta pAB}{\left[(\Delta pAB)^2 + p^2 C_{rit}\right]^{1/4}}, \tag{4}$$

where

$$A_s(p) = \begin{cases} A_{leak} \quad for\ p \le p_{crack} \\ A_{leak} + k\Delta(p - p_{crack})\ for\ p_{crack} < p < p_{max} \\ A_{max} \quad for\ p \ge p_{max} \end{cases}.$$

Here, k is the linear constant of proportionality, and P_{Ct} is the pressure difference between the laminar and turbulent flows. Under pressure differential conditions, P_{Ct} and k can be determined according to the following equations:

$$k = \frac{A_{Max} - A_{Leak}}{P_{Max} - P_{crack}}$$

$$P_{Ct} = \frac{\rho}{2}\left(\frac{R_e C_{rit}\gamma}{C_D D_H}\right)^2$$

Assuming a constant forward flow to the Q_A chamber from the Q_B chamber, the valve flow equation is expressed as

$$Q_v = \frac{Q_A + Q_B}{2} = C_d A_s \sqrt{\frac{2\left|P_{pA} - P_{pB}\right|}{\rho\left[\left(P_{pA} - P_{pB}\right)^2 + P_{cr}^2\right]^{1/4}}} - C_d A_s \sqrt{\frac{2}{\rho}} \frac{\Delta pAB}{\left[(\Delta pAB)^2 + p^2 C_{rit}\right]^{1/4}}. \quad (5)$$

The actuator is connected by the two-line chambers Q_A and Q_B with pressure valves, flow valves, and a bidirectional pump. The equation for the forward and return chambers in a single cylinder is shown below [5,19]:

$$\begin{cases} Q_{cA} = \frac{dV_1}{dt} + \frac{V_0 + A_A x}{\beta_e} * \frac{dP_A}{dt} \\ Q_{cB} = \frac{dV_2}{dt} - \frac{V_0 - A_B x}{\beta_e} * \frac{dP_B}{dt} \end{cases}. \quad (6)$$

Q_{cA} flows into the cylinder, and Q_{cB} flows out of the cylinder from the initial cylinder. In addition, A_A and A_B are the areas of the forward chamber and the return chamber in the cylinder, x is the displacement of the cylinder, V_o is the initial volume of the cylinder, and β_e is the bulk modulus of the hydraulic oil. V_1 and V_2 are the volumes of the cylinder chambers. The single cylinder flow represents the addition of the flows in the lines. This is expressed as:

$$Q_C = \left(A_t x_c + \frac{V_0}{2\beta_e} P_L + \frac{x_c}{2\beta_e} F_t\right)s, \quad (7)$$

where

$$\begin{cases} A_t = A_A + A_B \\ Q_C = \frac{Q_A + Q_B}{2} = A\dot{x}_c + \frac{V_0}{2\beta_e}\left(\frac{dP_A}{dt} - \frac{dP_B}{dt}\right) + \frac{A_A x}{2\beta_e}\dot{P_A} + \frac{A_B x}{2\beta_e}\dot{P_B} \\ F_t = F_A + F_B \end{cases}.$$

F_t is the total force on the chambers, and F_A and F_B are the forces from $\dot{P_A}$ and $\dot{P_B}$, respectively. Based on the equations of the pump flow, the cylinder flow, and the valve flow in the EHA circuit, the continuity equation for the forward chamber can be expressed as follows:

$$Q_p = Q_C + Q_v \quad (8)$$

$$D_{pv}\omega - C_t P_L = \left(A_t x_c + \frac{V_0}{2\beta_e} P_L + \frac{x_c}{2\beta_e} F_t\right)s + C_s A_s \sqrt{\frac{2\left|P_{pA} - P_{pB}\right|}{\rho\left[\left(P_{pA} - P_{pB}\right)^2 + P_{cr}^2\right]^{1/4}}} - C_d S \sqrt{\frac{2}{\rho}} \frac{\Delta pAB}{\left[(\Delta pAB)^2 + p^2 C_{rit}\right]^{1/4}} \quad (9)$$

There is an assumption that the system's pressure valve should be kept under the valve setting P_{set} of the two safety valves. Therefore,

$$D_{pv}\omega = \left(A_t x_c + \frac{V_0}{2\beta_e}P_L + \frac{x_c}{2\beta_e}F_t\right)s + C_s A_s \sqrt{\frac{2\left|P_{pA} - P_{pB}\right|}{\rho\left[\left(P_{pA} - P_{pB}\right)^2 + P_{cr}^2\right]^{1/4}}} + C_t P_L. \tag{10}$$

The plant dynamics of the force balance equation for the cylinder is expressed as follows:

$$P_L = \frac{Ms^2 x_c + Bs\, x_c + Kx_c + F_g}{A} \tag{11}$$

$$\begin{cases} F = (P_A - P_B)A = M\frac{d^2x_c}{dt^2} + B\frac{dx_c}{dt} + Kx_c + F_g \\ F_g = F_t \end{cases}.$$

Here, F, M, B, K, and F_g denote the force, mass, damping coefficient, spring coefficient, and disturbance, respectively. From Equation (11), the differential Equation (12) is derived as shown below:

$$\left(\frac{dP_A}{dt} - \frac{dP_B}{dt}\right) = \frac{M}{A}\dddot{x}_c + \frac{B}{A}\ddot{x}_c + \frac{K}{A}\dot{x}_c + \frac{F_t}{A}x_c. \tag{12}$$

During normal operation, the system pressure valves P_A and P_B should be kept under the valve setting P_{set} of the two safety valves. Therefore,

$$D_{pv} = k_p\phi, \tag{13}$$

where the Laplace transform applies:

$$x_c = \frac{\frac{k_p\phi\omega}{A_t} - \frac{C_S A_S}{A_t}\sqrt{\frac{2\left|P_{pA}-P_{pB}\right|}{\rho\left[\left(P_{pA}-P_{pB}\right)^2+P_{cr}^2\right]^{1/4}}} - \frac{F_t}{AA_t}\left(\frac{V_0}{2\beta_e}s + C_t\right)}{\left(\frac{V_0 M}{2\beta_e AA_t}\right)s^3 + \left(\frac{V_0 B}{2\beta_e AA_t} + \frac{C_t M}{AA_t}\right)s^2 + \left(1 + \frac{F_t}{2A_t\beta_e} + \frac{V_0 K}{2\beta_e AA_t} + \frac{C_t B}{AA_t}\right)s + \frac{C_t K}{AA_t}} \tag{14}$$

If $\frac{C_t B}{AA_t} \ll 1$ and$k$issufficiently small, the spring loads can be disregarded; that is, K = 0 and C_t are the total coefficients of the system, and B is the damping coefficient. A linear model of the pump, valve, and cylinder can be expressed as follows [6]:

$$x_c = \frac{\frac{k_p\phi\omega}{A_t} - \frac{C_S A_S}{A_t}\sqrt{\frac{2\left|P_{pA}-P_{pB}\right|}{\rho\left[\left(P_{pA}-P_{pB}\right)^2+P_{cr}^2\right]^{1/4}}} - \frac{F_t}{AA_t}\left(\frac{V_0}{2\beta_e}s + C_t\right)}{\left(\frac{V_0 M}{2\beta_e AA_t}\right)s^3 + \left(\frac{V_0 B}{2\beta_e AA_t} + \left(\frac{C_t M}{AA_t}\right)s^2 + \left(1 + \frac{F_t}{2A_t\beta_e}\right)s} \tag{15}$$

where

$$\begin{cases} \omega_n = \sqrt{\left(\frac{2\beta_e AA_t}{V_0 M}\right)}, \delta_n = C_t\sqrt{\left(\frac{\beta_e M}{AA_t V_0}\right)} + B\sqrt{\left(\frac{V_0}{2AA_t\beta_e M}\right)} \\ G_t = \left(1 + \frac{F_t}{2A_t\beta_e}\right) \end{cases}.$$

Due to the motor speed,

$$\frac{x_c}{\omega} = \begin{cases} \frac{\frac{k_p\phi G_t}{A}}{s\left(\frac{s^2}{\omega_n^2} + \frac{\delta_n}{\omega_n}s + 1\right)}, \omega > 0 \\ \frac{-\frac{k_p\phi G_t}{A}}{s\left(\frac{s^2}{\omega_n^2} + \frac{\delta_n}{\omega_n}s + 1\right)}, \omega < 0. \end{cases} \tag{16}$$

The proposed hydraulic circuit was tested to verify the performance of the pump-controlled EHA via Simscape Fluids in Figure 3. The experimental results were gained from the input with the sine wave and the parameters shown in Table 1. Before designing the controller, some work must be done to convert the transfer function of the EHA model to a state-space model. A third-order system with the transfer function is expressed as

$$\begin{cases} \dot{x}_1 = x_2 = \dot{x}_c \\ \dot{x}_2 = x_3 = \ddot{x}_c \\ \dot{x}_3 = \dddot{x}_c = \dfrac{2\beta_e A A_t}{V_0 M} \begin{pmatrix} \frac{k_p \phi_u}{A_t} - \left(\frac{V_0}{2\beta_e}\frac{B}{AA_t} + \frac{C_t M}{AA_t}\right) \\ -(1 + \frac{F_t}{2A_t\beta_e} + \frac{V_0 k}{2\beta_e A A_t} + \frac{C_t B}{AA_t})x_2 \\ -(\frac{C_t K}{AA_t})x_1 \\ -\left(\frac{C_s A_s}{A_t}\sqrt{\frac{2|P_{PA}-P_{PB}|}{\rho[(P_{PA}-P_{PB})^2+P_{cr}^2]^{1/4}}} - \frac{F_t}{AA_t}(\frac{V_0}{2\beta_e}s + C_t)\right) \end{pmatrix} \end{cases}, \tag{17}$$

where

$$\begin{cases} a_p = \frac{2\beta_e A k_p \phi u}{V_0 M} \\ b_p = \frac{2\beta_e}{V_0 M}(\frac{V_0 B}{2\beta_e} + C_t M) \\ c_p = \frac{2\beta_e A A_t}{V_0 M}(1 + \frac{F_t}{2A_t\beta_e} + \frac{V_0 K}{2\beta_e A A_t} + \frac{C_t B}{AA_t}) \\ d_p = \frac{2\beta_e C_t K}{V_0 M} \\ f_p = \frac{2\beta_e A}{V_0 M}(C_s A_S \sqrt{\frac{2|P_{PA}-P_{PB}|}{\rho[(P_{PA}-P_{PB})^2+P_{cr}^2]^{1/4}}} - \frac{C_t F_t}{A}) \end{cases}$$

In the pump-controlled EHA equation, the system has many model uncertainties at the beginning of the control operation due to the total leakage coefficient and the variable load. For example, the parameters M, A, A_t, A_s, and V_0 change with the variable loads in the single-load actuator, and the parameters β_e and ρ change when the oil temperature increases. For these reasons, the pump-controlled EHA system is considered to be a nonlinear system. Gradually increasing uncertainties can lead to inaccuracy or instability in the control system. Therefore, these nonlinear terms must be considered to minimize the effect of uncertainties when designing the controller.

3. Design of an Adaptive Sliding Mode Control Scheme

An adaptive sliding mode control scheme is developed in order to minimize the model uncertainties for the pump-controlled EHA system using Equation (17). From Equation (17), the state-space model is easily formed via

$$\dot{x} = \begin{bmatrix} 0 & 1 & 0 \\ 0 & 0 & 1 \\ -d_p & -c_p & -b_p \end{bmatrix} x + \begin{bmatrix} 0 \\ 0 \\ a_p \end{bmatrix} u \tag{18}$$

$$\mathrm{x}_c = \begin{bmatrix} -f_p & 0 & 0 \end{bmatrix} x + o \cdot u.$$

The EHA plant model equation is developed by a first-order differential equation from the equation below:

$$\dot{x}_3 = -b_p x_3 - c_p x_2 - d_p x_1 - f_p + a_p u. \tag{19}$$

Here, u is its input and is equivalent to ω, x is the plant output, and b_p, c_p, d_p, f_p, and a_p are constant, unknown plant parameters. Let the desired reference model equation be expressed by the first-order reference model:

$$\dot{x}_m = a_m \mathrm{r} - b_m \ddot{x}_m - c_m \dot{x}_m - d_m x_m - f_m \tag{20}$$

where r is the bounded reference signal, and $a_m, b_m, c_m, d_m,$ and f_m are constant parameters. During the first step of designing adaptive control, we use the following control law:

$$\begin{array}{rcl} u & = & \hat{u} \\ \hat{u} & = & \hat{a}_1 \mathrm{r} + \hat{a}_2 x_3 + \hat{a}_3 x_2 + \hat{a}_4 x_1 + \hat{a}_5 \end{array} \tag{21}$$

where $\hat{a}_1, \hat{a}_2, \hat{a}_3, \hat{a}_4,$ and $\hat{a}_5$ are the variable feedback gains. When we use the controller above (21) in the plant model equation above (19), the closed-loop dynamics become

$$\dot{x}_3 = -\left(b_p - a_p \hat{a}_2\right) x_3 - \left(c_p - a_p \hat{a}_3\right) x_2 - \left(d_p - a_p \hat{a}_4\right) x_1 - \left(f_p - a_p \hat{a}_5\right) + a_p \hat{a}_1 \mathrm{r}. \tag{22}$$

In this case, $\dot{x}_3$ is not a perfect model; hence, the tracking error is expressed as

$$\dot{e} = \dot{x}_3 - \dot{\hat{x}}_m. \tag{23}$$

If we know the EHA model parameters, $\hat{a}_1$, $\hat{a}_2$, $\hat{a}_3$, $\hat{a}_4$, and $\hat{a}_5$ are equal to a_1, a_2, a_3, a_4, and a_5, respectively. Estimation of the error parameter can be done using the adaptation law and the ideal parameters, $\tilde{a}_i = \hat{a}_i - a_i$. This is expressed as

$$\dot{e} = a_p \tilde{a}_2 x_3 + a_p \tilde{a}_3 x_2 + a_p \tilde{a}_4 x + a_p \tilde{a}_5 + a_p \tilde{a}_1 r \tag{24}$$

where

$$\begin{cases} a_1 = \frac{a_m}{a_p} \\ a_2 = \frac{b_p - b_m}{a_p} \\ a_3 = \frac{c_p - c_m}{a_p} \\ a_4 = \frac{d_p - d_m}{a_p} \\ a_5 = \frac{f_p - f_m}{a_p} \end{cases}.$$

Lemma 1 ([24]). *For adaptation laws, two signals Φ and e are considered. $\Phi(t)$ is a vector function of time, and v(t) is a measurable vector. If the vector Φ* chances according to

$$\dot{\Phi}(t) = -sgn(k)\gamma e v(t).$$

We apply Lemma 1 to obtain the adaptive law, and γ is a positive constant. Hence, e is globally bounded. As a result, the adaptive law can be expressed as follows:

$$\begin{cases} \dot{\hat{a}}_1 = -sgn\left(a_p\right)\gamma e r \\ \dot{\hat{a}}_2 = -sgn\left(a_p\right)\gamma e x_3 \\ \dot{\hat{a}}_3 = -sgn\left(a_p\right)\gamma e x_2 \\ \dot{\hat{a}}_4 = -sgn\left(a_p\right)\gamma e x_1 \\ \dot{\hat{a}}_5 = -sgn\left(a_p\right)\gamma e \end{cases}. \tag{25}$$

Let $\tilde{x}_o = x_c - x_d$ be the tracking error of variable x. Owing to the third degree of the EHA, the surface S (t) can be expressed as follows [24]:

$$\mathrm{S}(\mathrm{x};\mathrm{t}) = \left(\frac{d}{dt} + \lambda\right)^3 \int_0^t e(\tau)\mathrm{d}\tau = \ddot{e} + 3\lambda\dot{e} + 3\lambda^2 e + \lambda^3 \int_0^t e(\tau)\mathrm{d}\tau. \tag{26}$$

Taking the derivative S, we can determine the weighted sum of the position error and the velocity error:

$$\begin{aligned} \dot{S} &= \dot{x}_3 + u - \dot{\hat{x}}_m + 3\lambda\ddot{e} + 3\lambda^2\dot{e} + \lambda^3 e \\ \dot{S} &= \dot{e} + u + 3\lambda\ddot{e} + 3\lambda^2\dot{e} + \lambda^3 e. \end{aligned} \tag{27}$$

Substituting the error of the parameter estimation (24) into the sliding condition (27), the sliding condition then becomes

$$s\dot{S} = \mathrm{s}\Big(a_p\tilde{a}_2x_3 + a_p\tilde{a}_3x_2 + a_p\tilde{a}_4x + a_p\tilde{a}_5 + a_p\tilde{a}_1\mathrm{r} + 3\lambda\ddot{e} + 3\lambda^2\dot{e} + \lambda^3 e + u\Big) \le -\eta|s| \tag{28}$$

and the control law becomes

$$u = \hat{u} - k{\cdot}sat\left(\frac{s}{\phi}\right) \tag{29}$$

where

$$\hat{u} = -a_p\hat{\tilde{a}}_2x_3 - a_p\hat{\tilde{a}}_3x_2 - a_p\hat{\tilde{a}}_4x - a_p\hat{\tilde{a}}_1\mathrm{r} - a_p\hat{\tilde{a}}_5 - 3\lambda\ddot{e} - 3\lambda^2\dot{e} - \lambda^3 e.$$

Substituting the above control law (29) into the sliding condition (28) results in

$$s\left\{a_p\Big(\Big(\tilde{a}_2 - \hat{\tilde{a}}_2\Big)x_3 + \Big(\tilde{a}_3 - \hat{\tilde{a}}_3\Big)x_2 + \Big(\tilde{a}_4 - \hat{\tilde{a}}_4\Big)x_1 + \Big(\tilde{a}_1 - \hat{\tilde{a}}_1\Big)r + \Big(\tilde{a}_5 - \hat{\tilde{a}}_5\Big)\Big) + k{\cdot}sat\left(\frac{s}{\phi}\right)\right\} \le -\eta|s| \tag{30}$$

where

$$sat\left(\frac{s}{\phi}\right) = \begin{cases} +0.5 : \frac{s}{\phi} > 0 \\ -0.5 : \frac{s}{\phi} < 0 \end{cases}.$$

$\hat{a}_1, \hat{a}_2, \hat{a}_3, \hat{a}_4,$ and $\hat{a}_5$. are feedback gain parameters and lambda and k are the design parameters. $\frac{s}{\phi}$ is the boundary layer. When $\frac{s}{\phi}$ is inside the boundary layer, a saturation function is used to prevent any sudden change of u. At this stage, we analyze and demonstrate the stability of the system using the Lyapunov theory. We utilize the following Lyapunov function:

$$V = \frac{1}{2}e^2 + \frac{1}{2}\gamma^{-1}\Big(\tilde{a}_1^2 + \tilde{a}_2^2 + \tilde{a}_3^2 + \tilde{a}_4^2 + \tilde{a}_5^2\Big) \ge 0. \tag{31}$$

The derivative of V (32) becomes

$$\dot{V} = s[\Big(-a_p\hat{\tilde{a}}_2x_3 - a_p\hat{\tilde{a}}_3x_2 - a_p\hat{\tilde{a}}_4x_1 - a_p\hat{\tilde{a}}_1r - a_p\hat{\tilde{a}}_5 - k{\cdot}sgn(s)\Big) \le -\eta|s| \tag{32}$$

where

$$\begin{aligned} \dot{V} = s[&(-a_p\hat{\tilde{a}}_2x_3 - a_p\hat{\tilde{a}}_3x_2 - a_p\hat{\tilde{a}}_4x_1 - a_p\hat{\tilde{a}}_1r - a_p\hat{\tilde{a}}_5 - k\cdot sgn(s)) \\ &+\gamma^{-1}|a_p|\tilde{a}_1(\dot{\hat{a}}_1 + sgn(a_p)\gamma er) + \gamma^{-1}|a_p|\tilde{a}_2(\dot{\hat{a}}_2 + sgn(a_p)\gamma ex_3) \\ &+\gamma^{-1}|a_p|\tilde{a}_3(\dot{\hat{a}}_3 + sgn(a_p)\gamma ex_2) + \gamma^{-1}|a_p|\tilde{a}_4(\dot{\hat{a}}_4 + sgn(a_p)\gamma ex_1) \\ &+\gamma^{-1}|a_p|\tilde{a}_5(\dot{\hat{a}}_5 + sgn(a_p)\gamma e). \end{aligned}$$

Because the derivative of the Lyapunov function is less than zero, the adaptive sliding mode control scheme is globally stable. Figures 4 and 5 demonstrate that the proposed control reaches the target valve well after 2.5 s in Simulink.

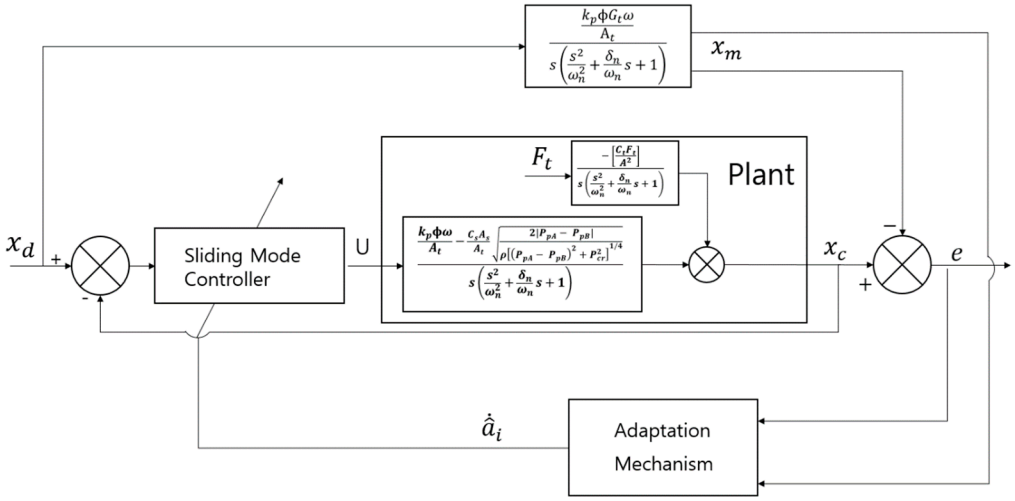

Figure 4. Adaptive sliding mode control scheme.

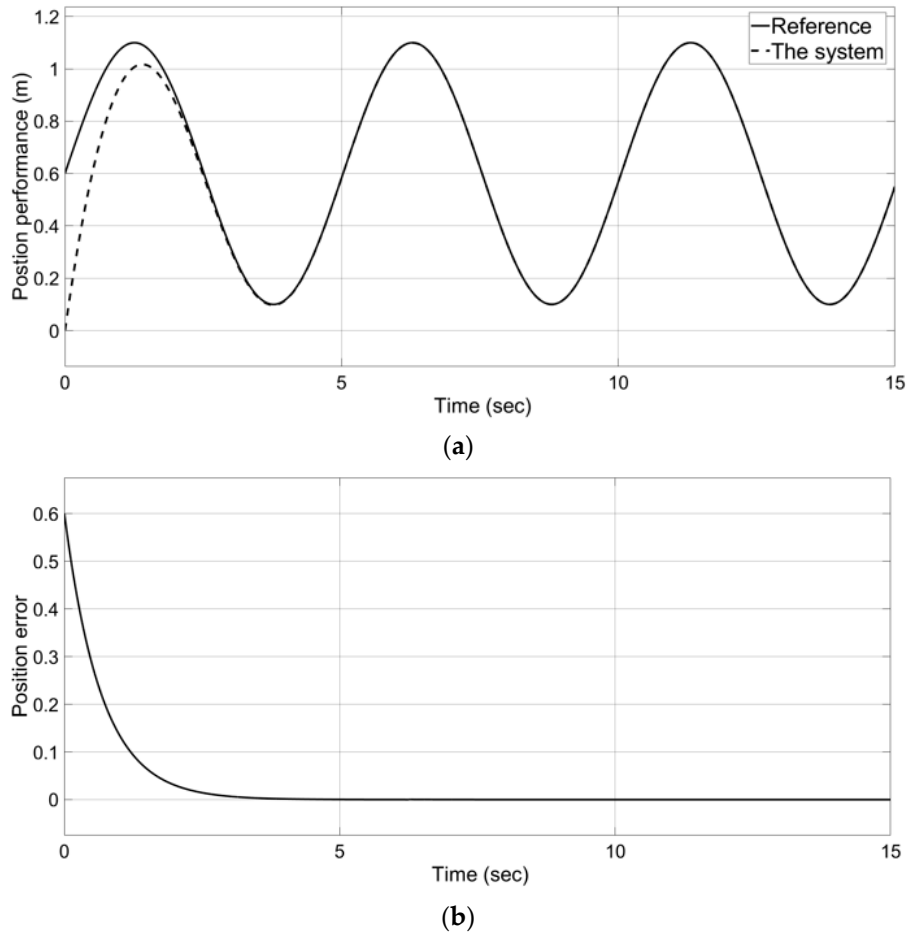

Figure 5. Simulation result of the adaptive sliding mode control scheme: (**a**) results of position performance and (**b**) error in the performance.

4. Experimental Results

To verify the proposed controller, the experimental setup shown in Figure 6 was used. The pump-controlled EHA system included the designed 0.8 cc swash axial piston pump, the modularized hydraulic circuit, a Gefran 125 mm linear displacement transducer, a 120 mm hydraulic cylinder, and a TI f28379d component as the main controller unit. The size of the pump is 5 cm in width, 6.8 cm in

length, and 5 cm in height. The modularized hydraulic circuit included two check valves, four pilot valves, two safety valves, and a tank for suction and draining. The maximum allowable pressure of the hydraulic cylinder was 3.5 Mpa. The size of the modularized block is 9 cm in width, 12 cm in length, and 10 cm in height. The system clock on the TI f28379d device was 200 MHz, and the system interruptions occurred at programmed intervals of 0.001 s. The 400 W Maxon motor was connected to the pump. The detailed hydraulic parameters for the experiment are shown in Table 2.

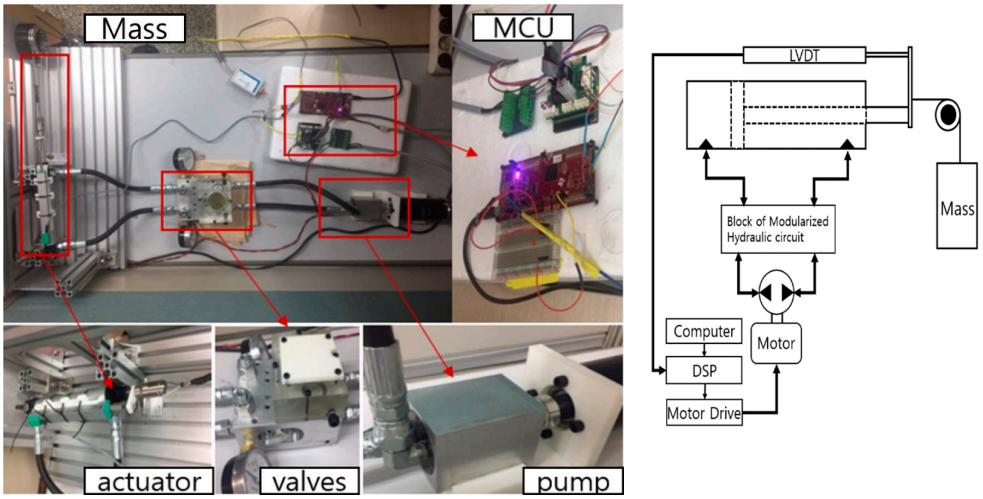

(**a**) (**b**)

Figure 6. (**a**) Experimental setup, including the bidirectional swash axial piston pump, the modularized circuit, actuators, the main controller unit (MCU), and (**b**) a schematic representation of the experimental setup.

Table 2. Hydraulic Parameters for the electro-hydraulic actuator (EHA) Experiment.

Component	Parameter	Specification	Component	Parameter	Specification
Hydraulic Cylinder	Bore size	20 mm	Modularized circuit	Safety valve operating pressure	24 bar
	Rod size	10 mm		Check valve cracking pressure	0.2 bar
	Maximum allowable pressure	3.5 Mpa		Pilot check valve cracking pressure	0.5 bar
	Stroke length	120 mm		Tank	100 mL
Hydraulic Pump	Cam angle	11°	LVDT	Full length	125 mm
	Displacement	0.8 cc	Weight	Mass	15 kg
	Operating pressure	30 kgf/cm^2	Motor	Input voltage	48 V
	Piston stroke	5 mm		Watts	400 W
	Piston numbers	7	MCU	System clock	200 MHz
	Piston diameter	5 mm	Hydraulic oil	Model	ISO VG 46
				Bulk modulus	15,000 bar

Figure 7 shows that the pump-controlled EHA system without a mass performed well. At the beginning of the experiment, we set the different start locations of the input value and desired value because we wanted to see how well and quickly the proposed system tracks the desired value. In the experiment, the design parameters of η, K, and lambda were set by 0.8, 0.35, and 10, respectively. The cylinder moved forward and backward by 10 cm at five-second intervals. The goal of the proposed controller shown in Figure 7a is to achieve suitable tracking to the sine wave reference, although it was inaccurate at the beginning of the control operation for two seconds. However, due to the rotational

moment of inertia and the pumped controlled characteristics, especially the slow response due to the large volume, it was difficult to track accurately and completely in this manner when changing the direction of the cylinder. Therefore, as shown in Figure 7b, errors of 2 mm above and below occurred in the repetitive error section. To reduce this type of error, the motor speed rpm in the plant command was considered, as shown in Figure 7c. Because the maximum allowable speed of the Maxon motor is 4800 rpm, a limit was set here, at 4000 rpm, to ensure the safety of the motor. When entering the adaptive sliding mode surface, the motor speed was maintained at 1500–1700 rpm. Figure 7d–h show the feedback gain parameters in cm units. At the beginning of the control operation, the system was unstable and was seen to change significantly. Subsequently, the system became stable and maintained a constant value.

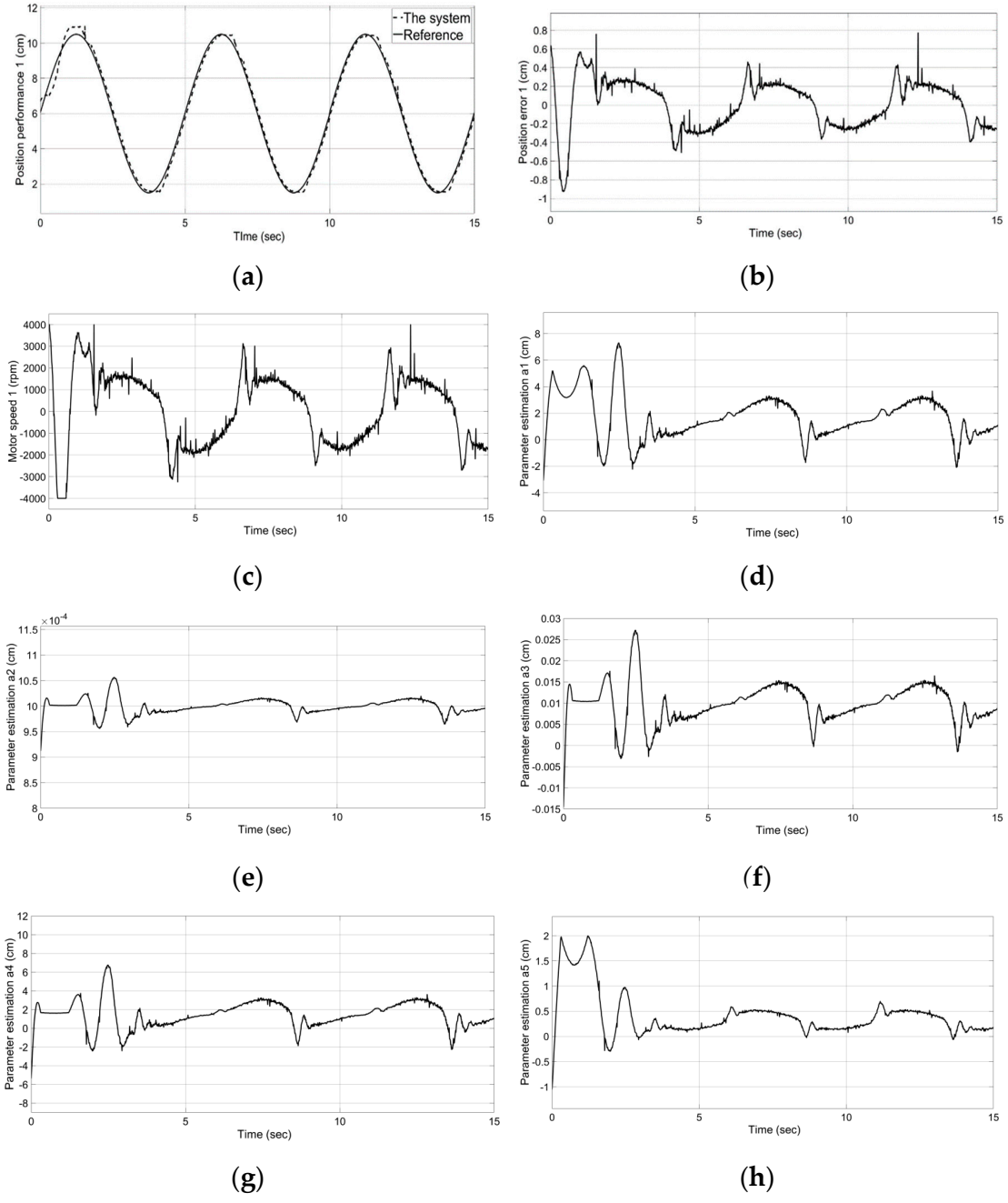

Figure 7. Experimental tracking responses without a load: (**a**–**c**) describe the EHA position performance in cm, the tracking error in cm, and the rpm of the motor; (**d**–**h**) are the estimation parameters in cm.

Figure 8 shows that the pump-controlled EHA system with the 15 kg mass performs well. We applied the same parameter gains shown in Figure 7 and confirmed the following results. Compared with Figure 7a, the system stabilization time of Figure 8a is delayed by two seconds. However, past that point, we confirmed that the system tracks the desired input well. Due to the moment of inertia by the mass, the instantaneous error of about 4 mm occurred at 11 s, as shown in Figure 8b. In addition, compared with Figure 7c, we confirmed that the motor speed increases due to the mass, as shown in Figure 8c. Figure 8d–h indicate that large fluctuations arise until the estimation parameters stabilize due to the mass.

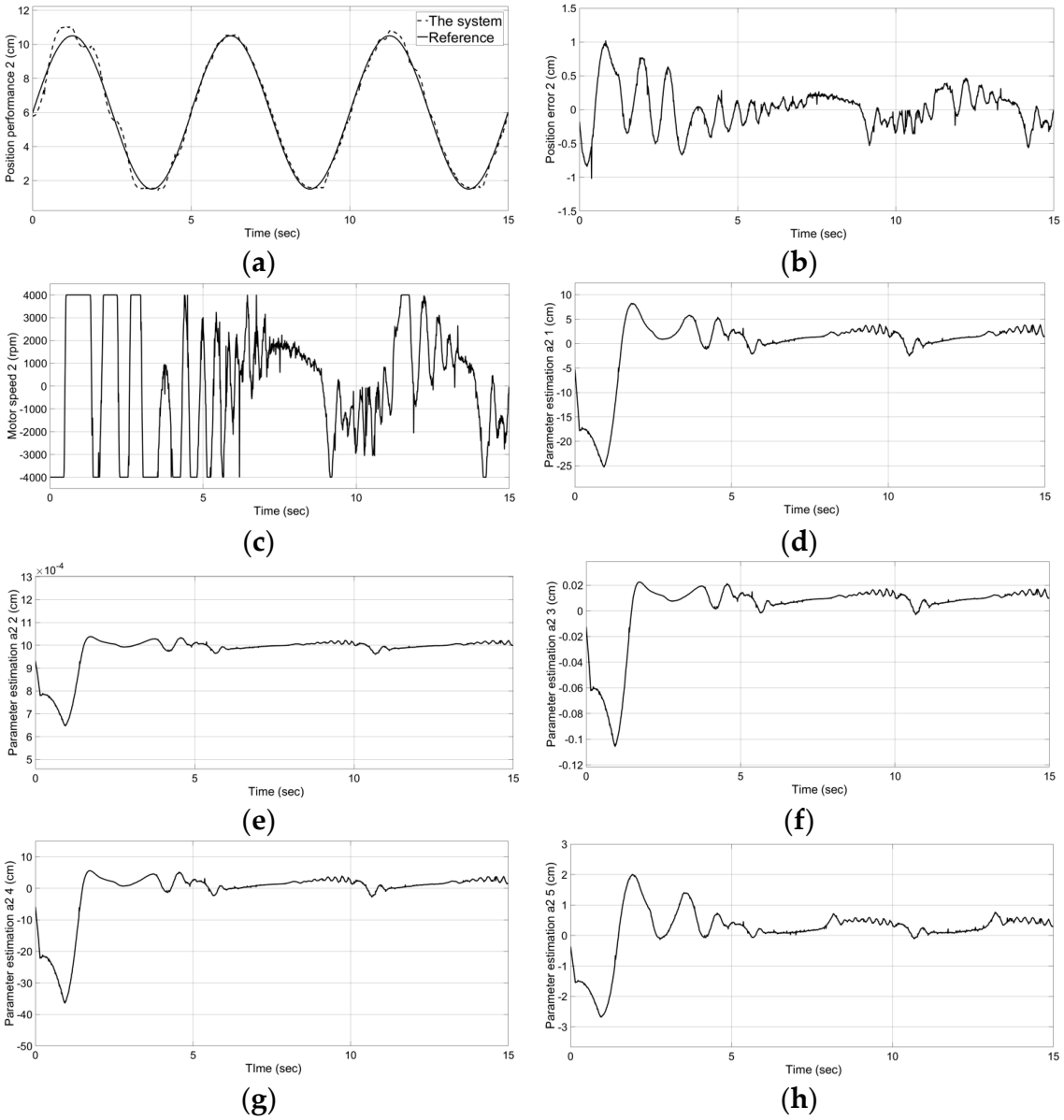

Figure 8. Experimental tracking responses with a 15 kg mass: (**a**–**c**) describe the position performance of the EHA in cm, the tracking error in cm, and the rpm of the motor. (**d**–**h**) are estimation parameters in cm.

5. Discussion

The proposed adaptive sliding mode control scheme was applied to a pump-controlled EHA. We found that the EHA system performance and estimation parameters varied depending on the designed parameters. As the lambda value increased, the system reached the desired input. However, as the

size of the value increased, the chattering problem occurred. When η was not overly small, we found that there was no significant difference in the performance of the EHA system. As the value of K increased, the system showed a quick response to find the target value. Based on this, experiments were conducted with and without a mass, and it was confirmed that an error occurred in a certain section in the absence of a mass. When the 15 kg mass was present, the error increased due to the gravity moment of the weight. Through the experimental results, the performance of the proposed adaptive sliding mode control scheme was verified to reach the target value accurately, despite the existence of model uncertainty. As a result, the proposed EHA is suitable for a wearable robot because of its compact size, safety, and high energy efficiency and accuracy.

Author Contributions: B.S. and D.L. contributed conceptualization, performed the experiments; B.S. designed the pump, hydraulic circuit, EHAs, controller, wrote the paper; S.Y.P. analyzed the data, reviewed and edited the paper; Y.S.B. contributed funding acquisition, supervision, project administration.

Funding: This research was supported by the Basic Science Research Program grant funded by the National Research Foundation of Korea (NRF) (No. 2017R1A2B4009265).

Conflicts of Interest: The authors declare no conflict of interest.

References

1. Yu, H.; Liu, Y.; Hasan, M.S. Review of modeling and remote control for excavators. *Int. J. Adv. Mechatron. Syst.* **2009**, *2*, 68–88. [CrossRef]
2. Xue, X.D.; Cheng, K.W.E.; Zhang, Z.; Lin, J.K.; Wang, D.H.; Bao, Y.J.; Wong, M.K.; Cheung, N. Study of Art of Automotive Active Suspensions. In Proceedings of the 4th International Conference on power Electronics Systems and Applications, Hong Kong, China, 8–10 June 2011.
3. Kim, J.H.; Shim, M.; Ahn, D.H.; Son, B.J.; Kim, S.Y.; Kim, D.Y.; Baek, Y.S.; Cho, B.K. Design of a Knee Exoskeleton Using Foot Pressure and Knee Torque Sensors. *Int. J. Adv. Robot. Syst. J. Robot.* **2015**, *12*, 112. [CrossRef]
4. Crimmins, E.M. Lifespan and Healthspan: Past, Present, and Promise. *J. Gerontol.* **2015**, *55*, 901–911. [CrossRef] [PubMed]
5. Merritt, H.E. *Hydraulic Control Systems*; Wiley Publisher: New York, NY, USA, 1967; pp. 65–157.
6. Rabie, G.M. Leakage in hydraulic spool valves. In Proceedings of the National Conference of Fluid Power, Philadelphia, PA, USA, 7–9 November 1978.
7. Eryilmaz, B.; Wilson, B.E. Combining Leakage and Orifice Flows in a Hydraulic Servo valve Mode. *J. Dyn. Syst. Meas. Control* **1999**, *12*, 576–579.
8. Raade, J.W.; Kazerooni, H. Analysis and Design of a Novel Hydraulic Power Source for Mobile Robots. *IEEE Trans. Autom. Sci. Eng.* **2005**, *2*, 226–232. [CrossRef]
9. Padovani, D.; Ketelson, S.; Hagen, D.; Schmidt, L. A self-Contained Electro-Hydraulic Cylinder with Passive Load-Holding Capability. *Energies* **2019**, *12*, 292. [CrossRef]
10. Chaudhuri, A.; Wereley, N. Compact hybrid electrohydraulic actuators using smart materials: A review. *J. Intell. Mater. Syst. Struct.* **2011**, *23*, 567–634. [CrossRef]
11. Yang, Y.; Zhao, D.; Ma, L.; Zhu, Q.; Huang, D. Backstepping trajectory tracking control of electro-hydraulic actuators of lower limb load exoskeleton. In Proceedings of the IECON 2016—42nd Annual Conference of the IEEE Industrial Electronics Society, Florence, Italy, 23–26 October 2016.
12. Guan, C.; Pan, S. Adaptive sliding mode control of electro-hydraulic system with nonlinear unknown parameters. *Control Eng. Pract.* **2008**, *16*, 1275–1284. [CrossRef]
13. Guan, C.; Pan, S. Nonlinear Adaptive Robust Control of Single-Rod Electro-Hydraulic Actuator with Unknown Nonlinear parameters. *IEEE Trans. Control Syst. Technol.* **2008**, *16*, 434–445. [CrossRef]
14. Won, D.; Kim, W.; Shin, D.; Chung, C.C. High-Gain Disturbance Observer-Based Backstepping Control with Output Tracking Error constraint for Electro-Hydraulic Systems. *IEEE Trans. Control Syst. Technol.* **2014**, *23*, 787–795. [CrossRef]
15. Choi, Y.Y.; Lee, K.H.; Beak, J.J.; Moon, H.; Choi, H.R.; Koo, J.C. Pressure Feedback Effects of Electro-Hydraulic Actuator System. In Proceedings of the 11th International Conference on Ubiquitous Robots and Ambient Intelligence (URAI 2014), Kuala Lumpur, Malaysia, 12–15 November 2014.

16. Lin, Y.; Shi, Y.; Burton, R. Modeling and Robust Discrete-Time Sliding-mode control Design for a Fluid power Electro-hydraulic actuator (EHA) system. *IEEE/ASME Trans. Mechatron.* **2013**, *18*, 1–10. [CrossRef]
17. Xinliang, L.; Shan, J.; Jing, Z.; Wang, X. Adaptive sliding mode position control of electro-hydraulic servo system with single-rod actuators. In Proceedings of the 2013 IEEE International Symposium on Robotic and Sensors Environments (ROSE), Washington, DC, USA, 21–23 October 2013.
18. Guo, Q.; Yu, T.; Jiang, D. High-gain observer-based output feedback control of single-rod electro-hydraulic actuator. *IET Control Theory Appl.* **2015**, *9*, 2395–2404. [CrossRef]
19. Ahn, K.K.; Chi, D.N.; Jin, M. Adaptive Backstepping Control of an Electrohydraulic Actuator. *IEEE/ASME Trans. Mechatron.* **2014**, *19*, 987–995. [CrossRef]
20. Dao, T.L.; Ahn, K.K. Grey Prediction Based Adaptive Sliding Mode Control for Electro-Hydraulic Actuator system. In Proceedings of the 15th International Conference on Control Automation and Systems (ICCAS), Busan, Korea, 13–16 October 2015.
21. Van Nguyen, T.; Ha, C. Sensor Fault-Tolerance Control Design for mini Motion Package Electro-hydraulic Actuator. *Processes* **2019**, *7*, 89. [CrossRef]
22. Grabbel, J.; Ivantysynova, M. An Investigation of Swash plate Control Concepts for Displacement Controlled Actuators. *Int. J. Fluid Power* **2005**, *6*, 19–36. [CrossRef]
23. Fang, X.; Quyang, X.; Yang, H. Investigation into the Effects of the Variable Displacement of Mechanism on Swash Plate Oscillation in High-Speed Piston Pumps. *Appl. Sci* **2018**, *8*, 658. [CrossRef]
24. Slotine, J.-J.E.; Li, W. *Applied Nonlinear Control*; Prentice-Hall Publisher: Upper Saddle River, NJ, USA, 1991; pp. 276–371.